Epitaxial 2D MoSe₂ (HfSe₂) semiconductor / 2D TaSe₂ metal v.d.Waals Heterostructures

Dimitra Tsoutsou, Kleopatra E. Aretouli, Polychronis Tsipas, Jose Marquez-Velasco, Evangelia Xenogiannopoulou, Nikolaos Kelaidis, Sigiava Aminalragia Giamini, and Athanasios Dimoulas*

National Center for Scientific Research "DEMOKRITOS", 15310, Athens, Greece

KEYWORDS: $TaSe_2$, molecular beam epitaxy, van der Waals heterostructures, $TaSe_2$/$MoSe_2$ metal/semiconductor heterostructure

Molecular beam epitaxy of 2D metal $TaSe_2$/2D $MoSe_2$ ($HfSe_2$) semiconductor heterostructures on epi-AlN(0001)/Si(111) substrates is reported. Electron diffraction reveals an in-plane orientation indicative of van der Waals epitaxy, while electronic band imaging supported by first principles calculations and x-ray photoelectron spectroscopy indicate the presence of a dominant prismatic 2H-$TaSe_2$ phase and a minor contribution from octahedrally coordinated $TaSe_2$ which is present in $TaSe_2$/AlN and $TaSe_2$/$HfSe_2$/AlN but not detectable in the $TaSe_2$/$MoSe_2$/AlN, indicating superior structural quality of $TaSe_2$ grown on $MoSe_2$. The $TaSe_2$ workfunction of 5.5 eV as measured by ultraviolet photoelectron spectroscopy matches very well the semiconductor

1

workfunctions implying that epi-$TaSe_2$ can be used for low contact resistance to $MoSe_2$ and $HfSe_2$ offering additionally chemical and structural compatibility with sharp interfaces.

INTRODUCTION

Atomically thin sheets of layered transition-metal dichalcogenides with the formula MX_2 (TMDs, M=Mo, W, V, Nb, Ta, Ti, Zr, Hf, Re and X=Se, S, Te) exhibit a wide variety of electronic properties, ranging from wide band-gap semiconductors to superconductors [1-2]. The crystallographic structure of MX_2 materials consists of covalently bound X-M-X sandwich layers, which are connected to each other by the weak so-called van der Waals (vdW) interaction. While most of the exciting properties of these materials have been demonstrated on small exfoliated flakes [3-5], the current trend is to synthesize them on large area substrates. Remarkable progress is reported by Metal Organic Chemical Vapor Deposition (MOCVD) [6] but molecular beam epitaxy (MBE) is an attractive alternative offering flexibility for a fast screening of TMDs. Van der Waals epitaxy using MBE has been pioneered by Koma and coworkers long time ago [7]. More recently, MBE growth [8-14] of $MoSe_2$, $HfSe_2$ and $ZrSe_2$ reveal very good van der Waals epitaxy of atomically thin continuous and uniform films on suitable cm-scale crystalline substrates.

Metallic 2D TMDs are studied less despite the fact that metal layers could have applications in nanoelectronics as TMDs device interconnects as well as in spintronics for use in spin Hall effect devices [15]. Tantalum diselenide ($TaSe_2$) is a metallic TMD and very early studies report the epitaxy of ultrathin (8-15 ML) films of layered $TaSe_2$ grown on Se-terminated GaAs(111) substrates by MBE, but characterization was limited to grazing incidence X-ray diffraction measurements (GIXRD) [16]. In another work

performed by the same team, TaSe$_2$ thin films were epitaxially grown on MoS$_2$, MoTe$_2$ and SnSe$_2$ substrates, and two unidentified phases were obtained at different substrate temperatures [17].

In its bulk form, TaSe$_2$ is among the most intensively studied TMDs [18] and is known to have several polytypes. The 2H-TaSe$_2$ polytype [19] (Figure 1) is the most stable phase at room temperature in bulk and has a trigonal prismatic Se-Ta-Se coordination in the double layer TaSe$_2$ unit cell. The octahedrally coordinated 1T-TaSe$_2$ phase with a single layer TaSe$_2$ unit cell (Figure 1), exhibits a nearly commensurate $p\left(\sqrt{13}\times\sqrt{13}\right)R13.89^o$ superstucture at RT. The effects of Charge Density Waves (CDW) present in 1T-TaSe$_2$, apart from the Low energy electron diffraction (LEED) superstructure include a characteristic splitting of the Ta 4f X-ray photoelectron spectroscopy (XPS) spectra [20-21], as well as of the Ta valence d$_z^2$ band [22]. In addition, there exist the mixed 4H$_b$ and 6R-TaSe$_2$ polytypes, where both trigonal and octahedral coordinations occur alternatively in the c direction [18].

In this paper, we propose 2D metal TaSe$_2$ as a metal contact to 2D semiconductors materials such as MoSe$_2$ and HfSe$_2$. It should be noted that for any viable 2D semiconductor TMD technology, good contacts are necessary, which are a big challenge at present. The motivation here is to grow the chemically compatible (both are selenide materials) 2D semiconductor layers and the 2D metal contact layers in a single epitaxial step maintaining the integrity of the interfaces. Moreover, the 2D diselenide metals have large workfunctions (>5 eV), matching the workfunctions of 2D diselenide

semiconductors better than other conventional element metals. Therefore, our approach here creates the prospect of 2D metal/semiconductor contacts with low contact resistivity.

EXPERIMENTAL SECTION

The technologically important Al-face 200nm-AlN(0001)/Si(111) wafers prepared by MOCVD were used as the substrate materials. High purity refractory metals Ta, Mo and Hf were evaporated in the MBE chamber from e-gun and Se from effusion cell, respectively. We employ two-step growth; first $TaSe_2$ is deposited at low temperature $T_g \sim$ 450 ^{o}C and high Se/Ta ratio ~15:1 to ensure sufficient incorporation of Se and avoidance of Se vacancy defects, followed by an *in-situ* post deposition annealing (PDA) in UHV at higher temperature (~ 650 ^{o}C) in order to improve crystallinity. Deposited samples were structurally and physically characterized by means of *in-situ* Reflection High Energy Electron Diffraction (RHEED), X-ray Photoelectron Spectroscopy (XPS), and Angle-Resolved Photoemission Spectroscopy (ARPES) techniques. XPS spectra were collected with a PHOIBOS 100 (SPECS) hemispherical analyzer, at a pass energy of 15 eV. The take-off angle was set at 37° relative to the sample surface. Gaussian-Lorentzian shapes (Voigt functions) were used for deconvolution of the recorded spectra after standard Shirley background subtraction ARPES measurements were carried out using a 2D CCD detector and a He excitation source with He I radiation at 21.22 eV. The energy resolution of the system was better than 40 meV. Photoelectrons emitted by the samples are measured in the energy distribution curve (EDC) mode with a with polar angle step of 1°. The Density–Functional Theory (DFT) calculations were performed using the Vienna Ab Initio Simulation Package [23] and projector-augmented waves. The generalized-gradient approximation (GGA) [24] with Perdew–Burke–Ernzerhof (PBE)

[25] parameterization was used as exchange correlation functional. To include vdW corrections, the semi-empirical DFT-D3 Grimme's method [26] was applied. Self-consistent force optimizations were performed until the Hellmann-Feynman force between the atoms converged to 5×10^{-5} eV/Å. In order to minimize interlayer atomic interactions, a 22 Å vacuum was applied above the $TaSe_2$ layer. The energy cutoff was set at 500 eV, while the Monkhorst-Pack scheme [24] with a k-point grid of 15x15x1 was chosen. Calculation of the band structure with and without SOC were performed. Using for these calculations k-mesh 31 k-point per symmetric line along KΓM direction.

RESULTS AND DISCUSSION

Epitaxial orientation probed by electron diffraction

The RHEED patterns recorded along the perpendicular $\begin{bmatrix}1\bar{1}0\end{bmatrix}$ azimuth for the MBE-deposited $TaSe_2$ samples, as well as for the AlN substrate are presented in Figure 2. The streaky RHEED patterns of 4 ML $TaSe_2$ deposited on all AlN, $HfSe_2$ and $MoSe_2$ templates indicate good surface atomic ordering of the deposited $TaSe_2$ films. In particular for the $HfSe_2$ and $MoSe_2$ cases the RHEED patterns further point out to the formation of well oriented 2D metal/semiconductor epitaxial layers, indicative of vdW epitaxy. It is also evident that the use of the $MoSe_2$ template yields improved crystallinity of the $TaSe_2$ layer as compared to the $HfSe_2$ template, a result that is in agreement with XPS data presented below. It should be noted at this point that there is a lattice mismatch (~ 10 %) between AlN and $TaSe_2$ (a_{AlN}=3.11 Å [11], a_{TaSe2}=3.43 Å [27]), which explains the streak position mismatch in the RHEED patterns of bare and $TaSe_2$-deposited AlN

surfaces (blue and red arrows, respectively). Since an (1x1) diffraction pattern, characteristic of hexagonal reciprocal space is observed, it is concluded that $2H\text{-}TaSe_2$ is the dominant phase on the surface. The possibility that the $1T\text{-}TaSe_2$ phase co-exists on the surface in large proportions could be excluded, since no superstructure characteristic [21] of $1T\text{-}TaSe_2$ CDW lattice distortions is observed in RHEED.

Electronic Band Structure Imaging by ARPES

The formation of a dominant $2H\text{-}TaSe_2$ phase in our MBE deposited samples is also being further supported by ARPES measurements. The electronic band imaging along high symmetry directions of the Brillouin zone of a 4 ML $TaSe_2/AlN$ is shown in Figure 3(a), along with first principles calculations for both the 2H and $1T\text{-}TaSe_2$ phases (Figures 3(b) and (c)). It is seen that ARPES measurements reveal metallic bands which are in agreement with our DFT calculations assuming a stable 2H trigonal prismatic phase. In particular, a broad band attributed to Ta 5d orbitals [22], is seen to cross the Fermi level in the experimental valence band spectra. Immediately below this band there exist bands due to the Se 4p contributions [22]. As seen in Figure 3(c), for $1T\text{-}TaSe_2$ the Se 4p orbital are predicted to disperse linearly very close to the Ta 5d orbitals crossing at the Γ-point near the Fermi level. In our experimental data, the Se and Ta orbitals are well separated, which is in agreement with the theoretical calculations of the $2H\text{-}TaSe_2$ phase (Figure 3(b)).

Phase Formation Studied by X-Ray Photoelectron Spectroscopy

The aforementioned RHEED and ARPES results indicate that well oriented trigonal prismatic 2H-TaSe$_2$ films can be epitaxially grown, on three different templates, namely AlN, MoSe$_2$ and HfSe$_2$. XPS measurements were employed at this point in order to investigate in more detail the phase composition, as well as the chemical stability of the 2D metal TaSe$_2$ with the AlN substrate as well as with the 2D semiconductors MoSe$_2$ and HfSe$_2$. The Ta bonding configuration of the 4 ML-thick TaSe$_2$/AlN, TaSe$_2$/HfSe$_2$ and TaSe$_2$/MoSe$_2$ structures, was investigated from the core level photoemission Ta 4f and Se 3d lines reported in Fig. 4 and 5, respectively. The Ta spectra were fitted using a doublet of Voigt functions corresponding to Ta 4f$_{7/2}$ and Ta 4f$_{4/2}$ components. Spin-orbit splitting and area ratio values of 1.91 eV and 4:3 were fixed for the fit. It should be noted at this point that in the case of pure 2H-TaSe$_2$ phase, the Ta 4f lineshapes are highly asymmetric, with clear shoulders on the high binding energy side of the main peaks [28-30]. These shoulders are typical of trigonal prismatic coordinated layers and they actually originate from excitations in the narrow conduction band [28]. It is inferred form Figure 4(a), that the experimental Ta 4f spectrum of the TaSe$_2$/MoSe$_2$ sample resembles very well those recorded for a pure 2H-TaSe$_2$ phase [29-30], and therefore we claim the MBE formation of a clean 2H-TaSe$_2$ phase in the case where TaSe$_2$ is grown on MoSe$_2$. In detail, three Ta 4f components are presented in the case of TaSe$_2$/MoSe$_2$ sample, which were all assigned to the 2H-TaSe$_2$ phase. The dominant peak at lower BE (23 eV) is associated with the main 2H-TaSe$_2$ Ta 4f photoelectron contribution, whereas the two remaining peaks at higher BE (23.6 eV and 24.2 eV) were necessary in order to reproduce the aforementioned conduction band peak. On the contrary, the Ta 4f lineshapes of the TaSe$_2$/HfSe$_2$ (Fig. 4(b) and TaSe$_2$/AlN (Figure 4(c)) structures appear to

be distorted compared to the $TaSe_2/MoSe_2$ case (Figure 4(a)). The analysis of Ta 4f XPS core levels indicates that other metastable polytype phases may be present in the materials albeit in reduced proportions compared to the dominant 2H phase. In particular, deconvolution of these peaks reveals two additional well separated (~0.6 eV) doublet contributions, which are shifted to higher binding energies by ~ 0.6 eV with respect to the position of the main $2H-TaSe_2$ peak. It should be noted here that the binding energy of the additional peaks is almost coincident with the energy of the peak assigned to the conduction band excitation. The formation of minor amounts of the octahedrally coordinated 1T phase could be justified on the basis of XPS spectra since two CDW-induced additional peaks, exhibiting a core level shift of ~0.65 eV are evidenced, corresponding to inequivalent Ta sites in the $1T-TaSe_2$ structure [21]. The possibility that the additional lower intensity peaks in the Ta4f spectra are due to Se deficiency [31] may be safely excluded since, in this case, a chemical shift to lower binding energies is expected rather than higher energies. Figure 5(a) presents the Se 3d spin doublet ($3d_{5/2}$ and $3d_{3/2}$) for the MBE-deposited $TaSe_2$ samples. A fixed spin-orbit splitting and area ratio of 0.86 eV and 2:3, respectively were used for the fit. The distinct Se chemical environments in the $TaSe_2/MoSe_2$ sample were assigned mainly to the presence of Se-Ta, Se-Mo bonds, as expected, as well to only minor Se-Se bonds. Again, an extra peak is being introduced in the Se3d spectra of the $TaSe_2/AlN$ and $TaSe_2/HfSe_2$ samples, attributed to the formation of a minor $TaSe_2$ phase other that the 2H. Overall, XPS measurements combined with RHEED and ARPES data indicate that a pure $2H-TaSe_2$ phase is formed on $MoSe_2$ while a mixed phase with a dominant 2H-TaSe2 component is formed on AlN or $HfSe_2$ substrates.

Workfunction measurements and band lineups

Obtaining low resistivity metal contacts on 2D semiconductors is a challenge [32]. To reduce the contact resistance, an appropriate 2D metal with a workfunction that creates a low Schottky barrier height with the 2D semiconductor must be chosen. From the low energy electron cut-off in in-situ UPS, shown in Figure 6(a), a work function of 5.4-5.5 eV is deduced for $TaSe_2$ which matches quite well the workfunction of $HfSe_2$ (5.5 eV) [12] and is close to the value of 5.1 eV measured for $MoSe_2$ [11]. The band alignment diagrams between the different layers are shown in Figure 5(b). It is seen that in the case of $TaSe_2/HfSe_2$ the Fermi levels perfectly line-up according to the electron affinity rule while in the case of $TaSe_2/$ $MoSe_2$ heterostructure there is only a small deviation, indicating that $TaSe_2$ could form low barrier/low resistivity contacts with $HfSe_2$ and $MoSe_2$ 2D semiconductors.

DISCUSSION AND CONCLUSIONS

In this work we showed that $TaSe_2$ and $TaSe_2$ /$MoSe_2$ ($HfSe_2$) heterostructures can be grown by MBE on AlN(0001)/Si(111) substrates with good structural quality at verified by RHEED and ARPES electronic band imaging. The material shows a dominant prismatic $2H-TaSe_2$ component which is also the most stable polytype at room temperature in bulk. There is evidence though by XPS that $TaSe_2$ directly grown on the AlN substrate contains a minor polytype component with different Ta-Se bonding as expected for example in octahedrally coordinated $TaSe_2$. The best candidate for the minority phase is the $1T-TaSe_2$ with octahedral coordination, but the lack of evidence for such a phase in ARPES or RHEED data is of concern. The most plausible explanation is

that the 1T phase, if present, is in very small quantities on the surface beyond the detection limit of the latter two techniques which are extremely surface sensitive. Alternatively, the assumed octrahedrally coordinated $TaSe_2$ may come from small amounts of 6R or $4H_b$ phases co-existing with the dominant 2H-$TaSe_2$. The former phases (6R and $4H_b$) consist of alternating layers with octahedral and prismatic coordination [18]. Given that the Ta 4f spectrum of the $4H_b$ phase consists of contributions from both the octahedrally coordinated and prismatic layers [33], the presence of $4H_b$ minority is compatible with our XPS data. The possible presence of $4H_b$ minority raises the question about possible observation of superstructure spots in RHEED due to CDW-associated lattice distortions. It has been shown before [34] that superstructure spots in $4H_b$ indeed could be observed at RT but with lower intensity compared to a pure 1T phase, which could explain in part the lack of evidence for such superstructures in our RHEED data. It is also concluded here, that $TaSe_2$ quality degrades when it is grown on $HfSe_2$/AlN, judging from an increased polytype minority phase detected from XPS and fuzzier RHEED spectrum. In contrast, $TaSe_2$ structural quality improves when it is grown on $MoSe_2$/AlN reducing to a pure 2H phase material and better crystalline quality compared to $TaSe_2$/$HfSe_2$/AlN as evidenced from XPS and RHEED. These results indicate that $TaSe_2$ is better compatible with $MoSe_2$ rather than $HfSe_2$. Nevertheless, the workfunctions match very well in the case of $TaSe_2$/$HfSe_2$ heterostructure (both measured at 5.5 eV) suggesting an optimal 2D metal/2D semiconductor junction, although the $TaSe_2$/$MoSe_2$ is not far from optimum too. To verify low contact resistivity though requires additional development for the fabrication of simple devices by employing selective etching of the metal layers with respect to the

2D metal underneath and proper mesa isolation of the devices by etching which is beyond the scope of this work.

AUTHOR INFORMATION

Corresponding Author

*a.dimoulas@inn.demokritos.gr

Author Contributions

The manuscript was written through contributions of all authors. All authors have given approval to the final version of the manuscript.

ABBREVIATIONS

TMD, transition-metal dichalcogenides; Metal Organic Chemical Vapor Deposition, MOCVD; Molecular Beam Epitaxy, MBE; van der Waals, vdW; Grazing incidence X-ray diffraction, GIXRD; Charge density waves, CDW; Low energy electron diffraction. LEED; X-ray photoelectron spectroscopy, XPS; Post-deposition annealing (PDA);

Reflection high energy electron diffraction, RHEED; Angle-resolved photoelectron spectroscopy, ARPES; Energy distribution curve, EDC; Perdew-Burke-Ernzerhof, PBE; Generalized-gradient approximation, GGA; Spin-orbit coupling (SOC);

References

(1) Wang, Q. H.; Kalantar-Zadeh, K.; Kis, A.; Coleman, J. N.; Strano, M. S. Electronics and Optoelectronics of Two-Dimensional Transition Metal Dichalcogenides. *Nat.Nanotech.* **2012**, 7, 699-712.

(2) Geim, A. K.; Grigorieva, I. V. Van der Waals Heterostructures. *Nature* **2013**, 499, 419-425.

(3) Radisavljevic, B.; Radenovic, A.; Brivio, J.; Giacometti, V.; Kis, A.; Single-Layer MoS_2 Transistors, *Nat. Nanotech.* **2011**, 6, 147-150.

(4) Liu, H.; Ye, P. D. MoS_2 Dual-Gate MOSFET with Atomic-Layer-Deposited Al_2O_3 as Top-Gate Dielectric. *IEEE Elec. Dev. Lett.* **2012**, 33, 546-548.

(5) Wang, H.; Yu, L.; Lee, Y.-H.; Shi, Y.; Hsu, A.; Chin, M. L.; Li, L.-J.; Dubey, M.; Kong, J.; Palacios, T. Integrated Circuits Based on Bilayer MoS_2 Transistors. *Nano Lett.* **2012**, 12, 4674-4680.

(6) Kang, K.; Xie, S.; Huang, L.; Han, Y.; Huang, P. Y.; Mak, K. F.; Kim, C.-J.; Muller, D.; Park, J. High-Mobility Three-Atom-Thick Semiconducting Films with Wafer Scale Homogeneity. *Nature* **2015**, 520, 656-660.

(7) Koma, A.; Yoshimura, K. Ultrasharp Interfaces Grown with Van der Waals Epitaxy. *Surf. Sci.***1985**, 174, 556-560.

(8) Zhang, Y.; Chang, T.-R.; Zhou, B.; Cui, Y.-T.; Yan, H.; Liu, Z.; Schmitt, F.; Lee, J.; Moore, R.; Chen, Y.; Lin, H.; Jeng, H.-T.; Mo, S.-K.; Hussain, Z.; Bansil, A.; Shen, Z.-X. Direct Observation of the Transition from Indirect to Direct Bandgap in Atomically Thin Epitaxial $MoSe_2$. *Nat. Nanotech.* **2014**, 9, 111–115.

(9) Yue, R.; Barton, A. T.; Zhu, H.; Azcatl, A.; Pena, L. F., Wang, J.; Peng, X.; Lu, N.; Cheng, L.; Addou, R.; McDonnell, S.; Colombo, L.; Hsu, J. W. P.; Kim, J.; Kim, M. J.; Wallace, R. M.; Hinkle, C. L. $HfSe_2$ Thin Films: 2D Transition Metal Dichalcogenides Grown by Molecular Beam Epitaxy. *ACS Nano* **2015**, 9, 474–480.

(10) Liu, H.; Jiao, L.; Yang, F.; Cai, Y.; Wu, X.; Ho, W.; Gao, C.; Jia, J.; Wang, N.; Fan, H.; Yao, W.; Xie, M. Dense Network of One-Dimensional Midgap Metallic Modes in Monolayer $MoSe_2$ and Their Spatial Undulations. *Phy. Rev. Lett.* **2014**, 113, 066105.

(11) Xenogiannopoulou, E.; Tsipas, P.; Aretouli, K. E.; Tsoutsou, D.; Giamini, S. A.; Bazioti, C.; Dimitrakopulos, G.P.; Komninou, Ph.; Brems, S.; Huyghebaert, C.; Radu, I. P. High-Quality, Large-Area $MoSe_2$ and $MoSe_2/Bi_2Se_3$ Heterostructures on AlN(0001)/Si(111) Substrates by Molecular Beam Epitaxy. *Nanoscale* **2015**, 7, 7896-7905.

(12) Aretouli, K. E.; Tsipas, P.; Tsoutsou, D.; Marquez-Velasco, J.; Xenogiannopoulou, E.; Giamini, S. A.; Vassalou, E.; Kelaidis, N. P.; Dimoulas, A. Two-Dimensional

Semiconductor $HfSe_2$ and $MoSe_2/HfSe_2$ Van der Waals Heterostructures by Molecular Beam Epitaxy. *Appl. Phys. Lett.* **2015**, 106, 143105.

(13) Tsipas, P.; Tsoutsou, D.; Marquez-Velasco, J.; Aretouli, K. E.; Xenogiannopoulou, E.; Vassalou, E.; Kordas, G.; Dimoulas, A. Epitaxial $ZrSe_2/MoSe_2$ Semiconductor v.d. Waals Heterostructures on Wide Band Gap AlN Substrates. *Microelectron. Eng.* **2015**, 147, 269-272.

(14) Lehtinen, O.; Komsa, H.-P.; Pulkin, A.; Whitwick, M. B.; Chen, M.-W.; Lehnert, T.; Mohn, M. J.; Yazyev, O. V.; Kis, A.; Kaiser, U.; Krasheninnikov, A. V. Atomic Scale Microstructure and Properties of Se-Deficient Two-Dimensional $MoSe_2$. *ACS Nano* **2015**, 9, 3274-3283.

(15) Neal, A. T.; Du, Y.; Liu, H.; Ye, P. D. Two-Dimensional $TaSe_2$ Metallic Crystals: Spin–Orbit Scattering Length and Breakdown Current Density, *ACS Nano* **2014**, 8, 9137-9142.

(16) Shimada, T.; Nishikawa, H.; Koma, A.; Furukawa, Y.; Arakawa, E.; Takeshita, K.; Matsushita, T. Polytypes and Crystallinity of Ultrathin Epitaxial Films of Layered Materials Studied with Grazing Incidence X-ray Diffraction. *Surf. Sci.* **1996**, 369, 379-384.

(17) Shimada, T.; Ohuchi, F. S.; Parkinson, B. A. Epitaxial Growth and Charge Density Wave of $TaSe_2$. *Mat. Res. Soc. Symp. Proc.* **1992**, 230, 231.

(18) Wilson, J.A.; Yoffe, A. D. The Transition Metal Dichalcogenides Discussion and Interpretation of the Observed Optical, Electrical and Structural Properties. *Adv. Phys.* **1969**, 18, 193-335.

(19) Momma, K.; Izumi, F. VESTA 3 for Three-Dimensional Visualization of Crystal, Volumetric and Morphology Data. *J. Appl. Crystallogr.* **2011**, 44, 1272-1276.

(20) Wertheim, G. K.; DiSalvo, F. J.; Chiang, S. Charge-Density Waves and Many-Body Effects in X-Ray Photoelectron Spectroscopy of Layer-Structure Chalcogenides. *Phys. Rev. B* **1976**, 13, 5476.

(21) Horiba, K.; Ono, K.; Oh, J. H.; Kihara, T.; Nakazono, S.; Oshima, M.; Shiino, O.; Yeom, H. W.; Kakizaki, A.; Aiura, Y. Charge-Density Wave and Three-Dimensional Fermi Surface in $1T-TaSe_2$ Studied by Photoemission Spectroscopy. *Phys. Rev. B* **2002**, 66, 073106.

(22) Bovet, M.; Popovic, D.; Clerc, F.; Koitzsch, C.; Probst, U.; Bucher, E.; Berger, H.; Naumovic, D.; Aebi, P. Pseudogapped Fermi Surfaces of $1T-TaS_2$ and $1T-TaSe_2$: A Charge Density Wave Effect. *Phys. Rev. B* **2007**, 69, 125117.

(23) Perdew, J. P.; Wang, Y. Accurate and Simple Analytic Representation of the Electron-Gas Correlation Energy. *Phys. Rev. B: Condens. Matter Mater. Phys.* **1992**, 45, 13244.

[24] J. P. Perdew, K. Burke, and M. Ernzerhof, Generalized Gradient Approximation Made Simple, Phys. Rev. Lett. 77, 3865 (1996).

(25) Grimme, S.; Antony, J.; Ehrlich, S.; Krieg, S. A Consistent and Accurate Ab Initio Parametrization of Density Functional Dispersion Correction (DFT-D) for the 94 Elements H-Pu. *J. Chem. Phys.* **2010**, 132, 154104.

(26) Chadi, D. J.; Cohen, M. L. Special Points in the Brillouin Zone. *Phys. Rev. B: Condens. Matter Mater. Phys.* **1973**, 8, 5747.

(27) Sharma, S.; Auluck, S.; Khan, M. A. Optical Properties of 1T and 2H Phases of TaS_2 and $TaSe_2$. *Pramana Journal of Physics* **2000**, 54, 431-440.

(28) Hughes, H. P.; Scarfe, J. A. Lineshapes in Core-Level Photoemission from Metals: II. $2H\text{-}TaS_2$ and its Transition Metal Intercalates. J. *Phys. Condens. Matter* **1996**, 8, 1439-1455.

(29) Crawack, H.J.; Pettenkofer, C. Calculation and XPS Measurements of the Ta4f CDW Splitting in Cu, Cs and Li Intercalation Phases of $1T\text{-}TaX_2$ (X=S, Se). *Solid State Commun.* **2001**, 118, 325-332.

(30) Brauer, H. E.; Starnberg, H. I.; Holleboom, L. J.; Hughes, H. P.; Strocov, V. N.; Na and Cs Intercalation of $2H\text{-}TaSe_2$ Studied by Photoemission. *J. Phys. Condens. Matter* **2001**, 13, 9879-9895.

(31) McDonnell, S.; Addou, R.; Buie, C.; Wallace, R. M.; Hinkle, C. L. Defect-Dominated Doping and Contact Resistance in MoS_2. *ACS Nano* **2014**, 8, 2880-2888.

(32) Kappera, R.; Voiry, D.; Yalcin, S. E.; Branch, B.; Gupta, G.; Mohite, A. D.; Chhowalla, M. Phase-Engineered Low-Resistance Contacts for Ultrathin MoS_2 Transistors. *Nat. Mater.* **2014**, 13 1128-1134.

(33) Hughes, H. P.; Scarfe, J. A.; Lineshapes in core-level photoemission from metals: III. Site-dependent screening in the charge density wave materials 1T and 4Hb-TaS2, *J. Phys. Condens. Matter* **8**, (1996) 1457-1743

(34) Moret, R.; Tronc, E.; Atomic displacements in the charge-density wave induced superstructure of $4H_b$-$TaSe_2$, *Phil. Mag. B* **40**, (1979) 305-315
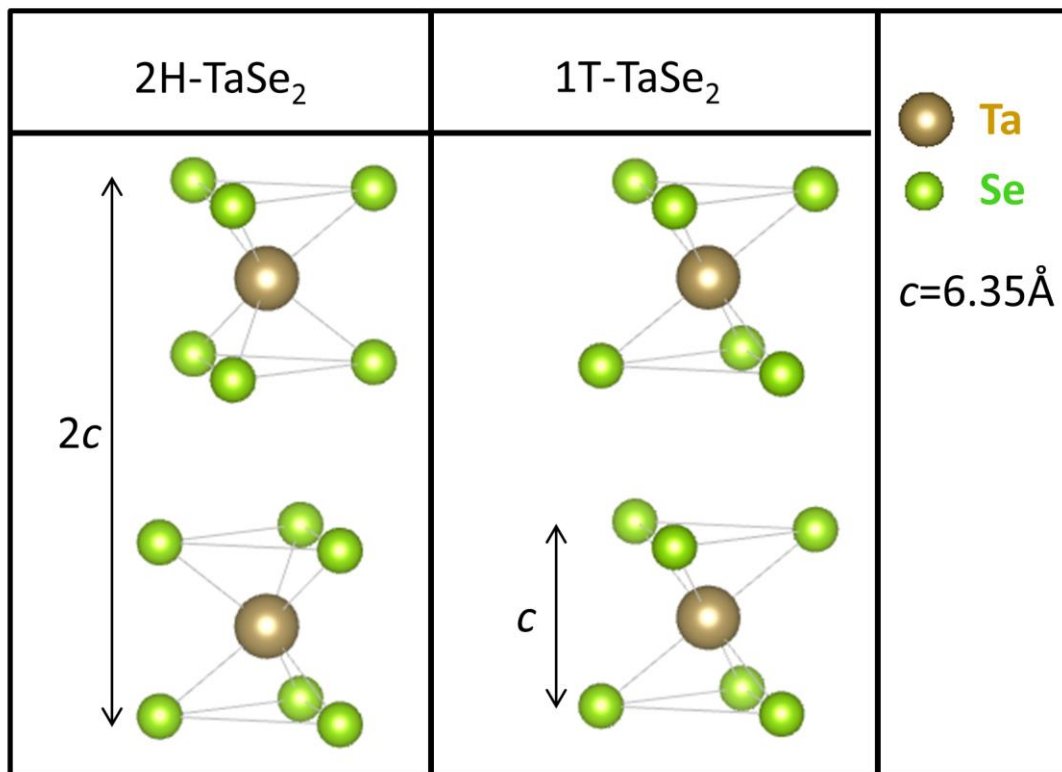
Figure 1. The crystallographic structure of the two most common 2H and 1T-TaSe$_2$ polytypes. The Se-Ta-Se coordination is trigonal prismatic in the 2H structure and octahedral in the 1T structure.
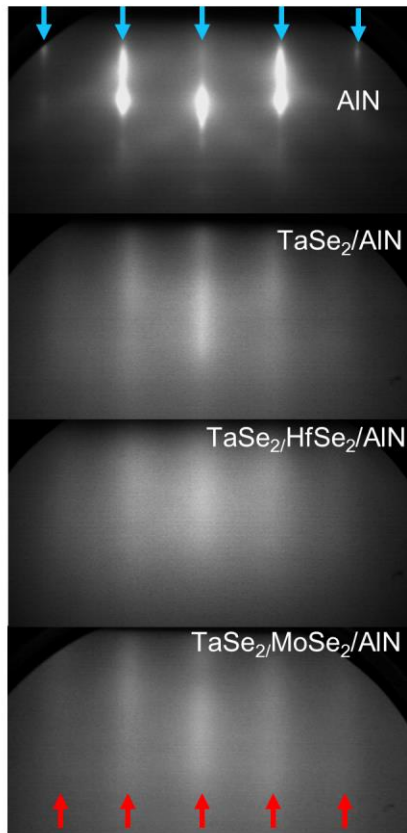
Figure 2. (a) RHEED diffraction patterns of the 4 ML MBE-deposited TaSe$_2$ films on different templates (AlN, HfSe$_2$ and MoSe$_2$) obtained along the $[1\bar{1}0]$ azimuth of the bare AlN(0001) surface, showing good quality epitaxial growth with excellent alignment of the 2D metal with the substrate. Blue and red arrows indicate the diffraction streaks of AlN(0001) and TaSe$_2$ superstructures, respectively.
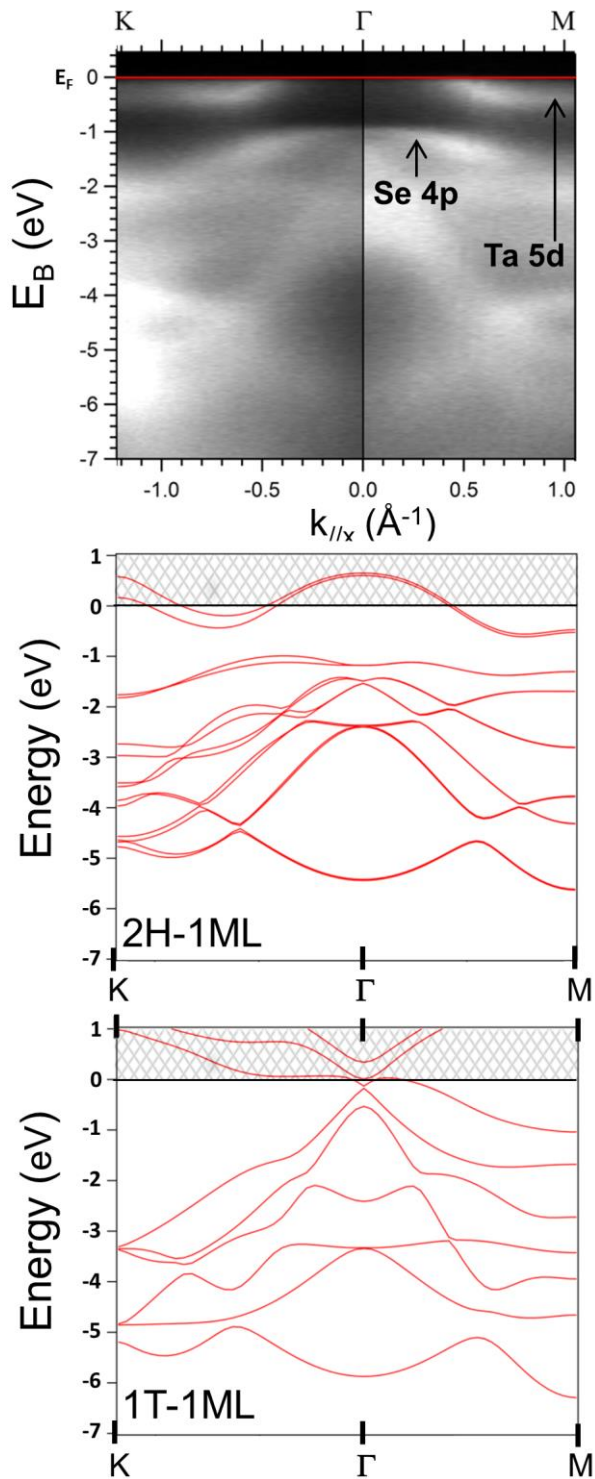
Figure 3. Band structure imaging by *in-situ* ARPES of 4 ML-TaSe$_2$/AlN (top) and DFT

bandstructure calculations for 2H (middle) and 1T (bottom) TaSe$_2$ phases. Experimental

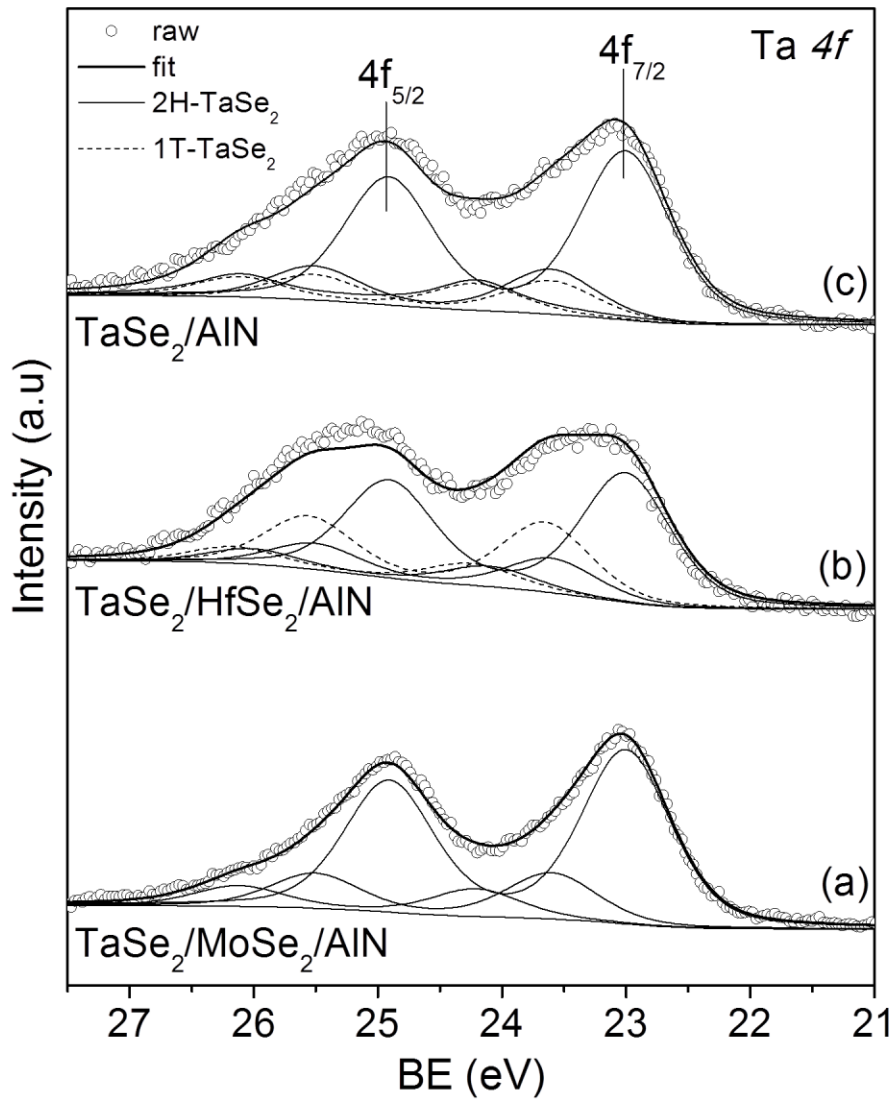data agree well with the formation of the trigonal prismatic 2H-TaSe$_2$ phase.
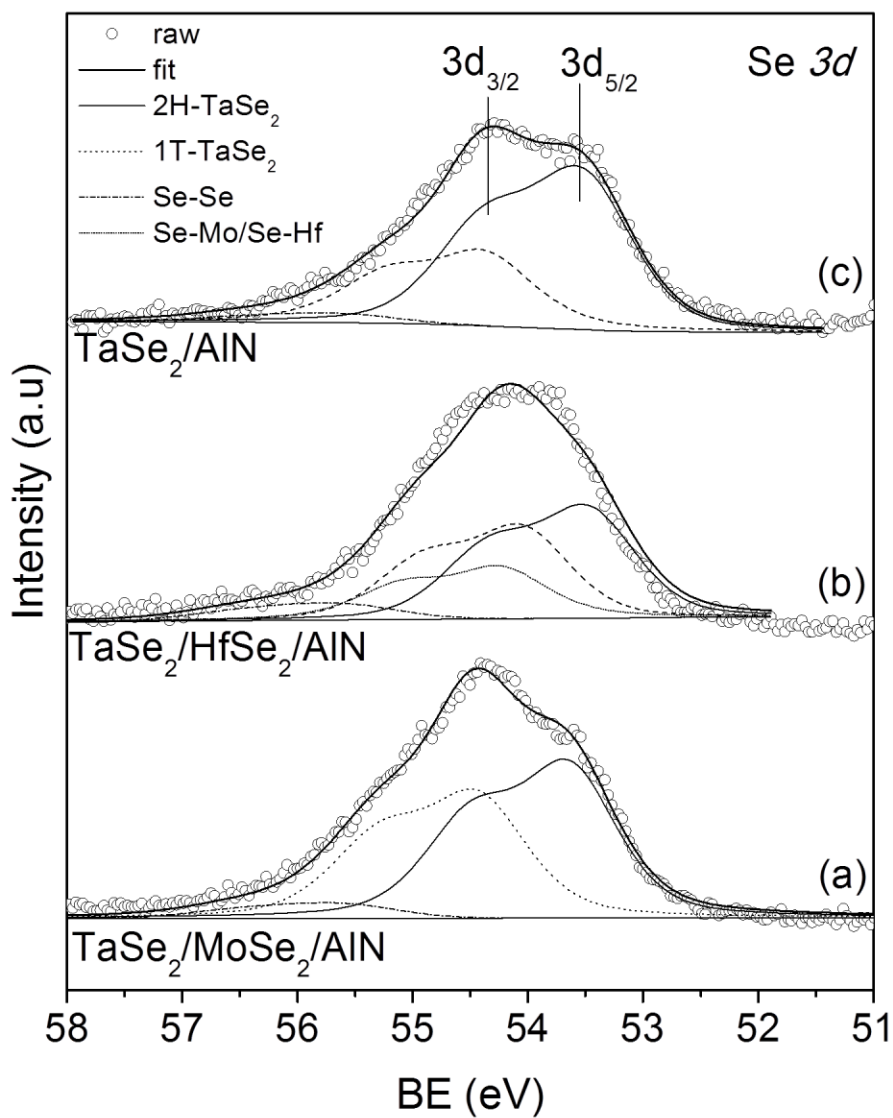
Figure 4. Deconvolution of the Ta 4f doublets of the 4-ML thin $TaSe_2$ films grown epitaxially on (a) $MoSe_2$, (b) $HfSe_2$ and (c) AlN templates, showing the formation of a pure (a)/dominant (b) and (c) $2H\text{-}TaSe_2$ phase in all cases.

Figure 5. Deconvolution of the Se 3d doublets of the 4-ML thin $TaSe_2$ films grown epitaxially on (a) $MoSe_2$, (b) $HfSe_2$ and (c) AlN templates, showing the formation of a pure (a)/dominant (b) and (c) 2H-$TaSe_2$ phase in all cases.
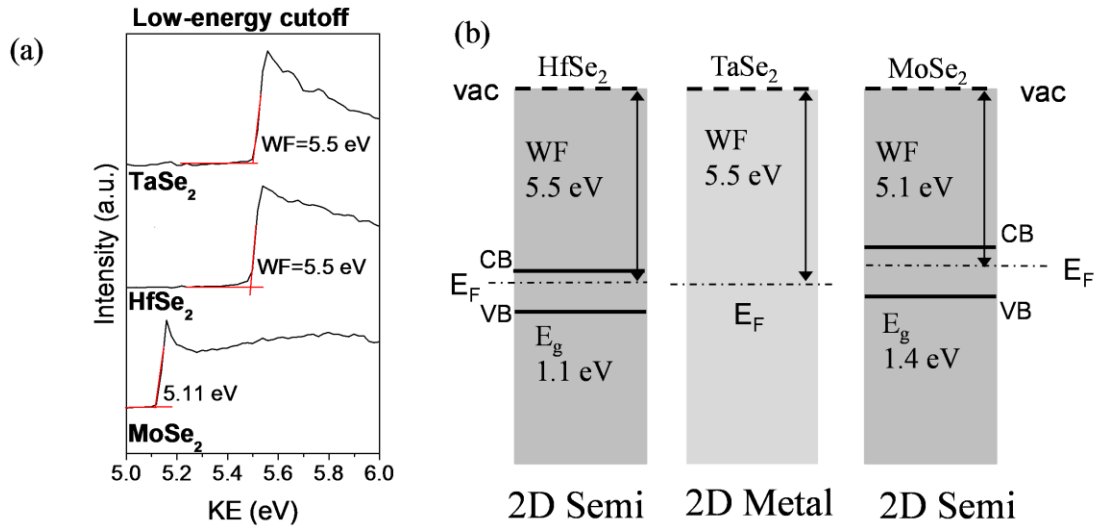
Figure 6. (a) Low energy cut off for TaSe$_2$, HfSe$_2$ and MoSe$_2$ samples, as determined from UPS measurements, (b) Schematic of the HfSe$_2$/TaSe$_2$ and MoSe$_2$/TaSe$_2$ band alignments as derived from UPS measurements, showing workfunction matching according to the electron affinity rule.

Graphical Abstract